PAPER

Check for updates

Reproducible 2D $Ti_3C_2T_x$ for perovskite-based photovoltaic device†

Qingchao Shen, [ID] * Chaoran Chen, Jiao Long and Saili Wang

$Ti_3C_2T_x$ (T_x denotes terminal group), resulting from two-dimensional (2D) Mxenes, has attracted significant attention due to energy shortage and catalysis. Herein, we present reproducible 2D $Ti_3C_2T_x$ obtained from commercial bulk Ti_3AlC_2 using a cost-effective and environment-friendly approach. Both etching and exfoliation processes were investigated with the rational selection of etchant, reaction time and exfoliation solution. The hydrofluoric acid (HF) etchant plays a key role in the production of 2D $Ti_3C_2T_x$ and therefore the recycling of HF is addressed for reproducible 2D MXenes. Hazardous HF waste was also neutralized *via* CaF_2 precipitation according to the regulations for HF sewage. Equally important, dimethyl sulfoxide (DMSO) was employed to promote the exfoliation of multilayer $Ti_3C_2T_x$ MXenes into $Ti_3C_2T_x$ nanosheets in an aqueous solution, which can couple with terminal groups and protect the exfoliated single-layers from recombination, facilitating interface passivation toward perovskite solar devices. The resulting perovskite solar cell exhibited striking improvements to achieve champion efficiency, with a PCE of 19.11%, which accounts for ~9% enhancement as compared to pristine devices.

Introduction

Mxenes, as new members of the 2D material family, have been attracting increasing attention since their discovery in 2011.[1,2] MXenes have the conventional formula of $M_{n+1}X_nT_x$, where $n = 1, 2,$ or 3; M is an early transition metal, commonly Ti, V, Cr, Nb, Ta, Zr, and Mo; X is C or N, and T_x denotes the terminating group –F, –OH, and =O.[3–7] Mxenes are brought about by layered ternary metal MAX *via* selectively etching the A element (typically, Al, Sn, Si or Ga) from their ternary carbide precursors.[8–11] To date, over 20 kinds of MXenes have already been discovered, and importantly, 2D materials prepared by the etching approach have fueled more MXene species. MXenes are famous for their high specific surface areas, rigid 2D layer structure, as well as excellent electronic properties, which have delivered numerous applications in energy storage, electronics, gas separation and catalyst field. There are over thousand reports per year on novel 2D MXene materials for supercapacitors,[12–15] batteries,[16–21] electronics[22,23] and detector sensors.[24–27] 2D titanium carbide ($Ti_3C_2T_x$) was the first synthesized MXene and is widely studied for energy storage. It not only exhibits excellent conductivity of 6500 S cm^{-1} for electrodes, but the robust 2D structure also serves as a host coupling with functional compounds for more applications.[28–31] Due to $Ti_3C_2T_x$ structure

School of Electronic Information and Electrical Engineering, Anyang Institute of Technology, Avenue West of Yellow River, Anyang 455000, China. E-mail: shenqingchao6688@ayit.edu.cn; tinglima@life.kyutech.ac.jp; Fax: +88-093-695-60; Tel: +88-093-695-6045

† Electronic supplementary information (ESI) available. See DOI: https://doi.org/10.1039/d2ra08088e

modification and abundant terminal groups, about a hundred papers were published in the energy field in 2021. Therefore, it is necessary to establish a common routine for the cost-effective production of 2D $Ti_3C_2T_x$ to support its deployment.

To date, the preparation of $Ti_3C_2T_x$ MXenes is heavily dependent on the hydrofluoric acid etching of bulk Ti_3AlC_2 from commercial or lab-made Ti_3AlC_2. The etchant, which may include LiF, NH_4F, FeF_3, and NH_4HF_2 in aqueous medium, reacts with A-site metals (for example, Al) to produce a 2D structure by releasing hydrofluoric acid in the etching process.[32–36] Through simply shaking or sonication, the $Ti_3C_2T_x$ can be delaminated into predominant nanosheets with a single layer, forming a single-layer nanosheet suspension.[37–40] HF solution is notorious for its toxicity and corrosivity, which requires strict implementation of sewage disposal. In this regard, the recycling and disposal of HF solution are important to achieve the reproduction of 2D $Ti_3C_2T_x$ for broadened applications.

In this paper, we present fundamental research including etchants, DMSO-assisted exfoliation, and the recycling of HF solution to produce 2D $Ti_3C_2T_x$ from the commercial Ti_3AlC_2 powder. There is a time-dependent transformation from the bulk to nanosheet structure in SEM images, along with the shifting of the XRD peaks. It was found that Ti_3AlC_2 was successfully etched in HF solution at room temperature for 12 hours, giving an accordion-like morphology with a high specific surface area. More importantly, the HF solution was recycled to reduce the HF quota, breaking through the limitations of sewage pollution for practical applications. DMSO-assisted exfoliation is beneficial to the stability of $Ti_3C_2T_x$ nanosheets,

yielding a uniform suspension with shelf storage for over 7 days. This study offers a routine for producing 2D $Ti_3C_2T_x$ in large batches from commercial Ti_3AlC_2, as well as highlighting the disposal of toxic HF and thus advancing the development of MXenes without the limitation of sewage pollution. $Ti_3C_2T_x$ nanosheets with functional terminal groups were deposited at the interface between the perovskite and charge transport layer, boosting the efficiency and stability of perovskite working devices.

Experimental section

Materials

The bulk Ti_3AlC_2 powder was obtained from Forsman Scientific (Beijing) Co. Ltd. China. The physical properties were measured and are listed in Table S1.† All of the glassware used in the following procedures were cleaned by sonication for 15 min in deionized water. HF (48%) and HCl (36%) were obtained from Wako, Japan (the concentration of HF determined by neutralization was 24.5 mol L^{-1}). NH_4F and LiF were obtained from Aihehua Agent Co. Ltd. N,N-dimethylformamide (DMF), chlorobenzene (CB) and dimethyl sulfoxide (DMSO) were obtained from Sigma Aldrich, Shanghai. Formamidinium iodide (FAI), methylammonium bromide (MABr), and cesium iodide (CsI), poly(3-hexylthiophene-2,5-diyl) (P3HT), lead(II) iodide (PbI_2), and lead bromide ($PbBr_2$) were purchased from Xi'an Polymer Light Technology Corp. SnO_2 colloid precursor (15 wt% in water) was purchased from Alfa Aesar. ITO glass was obtained from Liaoning Youxuan New Energy Technology Co. Ltd. All chemicals were used without any further purification. All chemicals used in the study were analytical grade.

Analysis

The residual H^- concentration was calculated through acid-base neutralization. The F^- ion concentration was determined by ion chromatography (Metrohm, Swiss). The morphology of $Ti_3C_2T_x$ was observed by scanning electronic microscopy (SEM, Electron Optics Co., Japan). The size distribution in suspension was carried out by dynamic light scattering (DLS, Malvern, UK). The crystallization of the prepared powder and films was determined *via* X-ray diffraction (Bruker D8 Advance) (Cu Kα radiation ($\lambda = 1.5418$ Å), 45 kV and 200 mA). The steady-state PL and time-resolved PL (TRPL) decay were measured using an integrated confocal microscopy system (Tau-3-P) with a laser excitation source. The current–voltage (J–V) curves were measured with a solar simulator and a Keithley 2400 source meter. The intensity of light irradiation was calibrated with a standard Si photodetector and adjusted to a light intensity of 1 sun (100 mW cm^{-2} AM1.5G). The active area was regulated to 0.09 cm^2 with a mask.

Methods

Etching of Ti_3AlC_2 MAX

$Ti_3C_2T_x$ were prepared by the acidic etching of the corresponding Ti_3AlC_2 (Forsman, Beijing) phases in a fluoride-containing aqueous solution. We employed 10 mL of HF (48%), NH_4F/HCl (10 M/10 M), and LiF/HCl (10 M/10 M) for the etching of Al from 1.0 g Ti_3AlC_2 in this work. For the HF and LiF/HCl etchant, the reaction temperature was held at room temperature under constant stirring for 24 h. For the NH_4F/HCl etchant, the hydrothermal reaction temperature was maintained at 150 °C for 24 h. After the reaction, the solution was centrifuged at 4000 rpm for 5 min, and the supernatant was decanted. These processes were repeated several times until the pH of the supernatant reached 6. The etched powder was washed with deionized (DI) water. The sediment was collected and labeled as HF, NH_4F/HCl and LiF/HCl, respectively.

Recycling and disposal of the HF etchant solution

The reuse of the HF solution is described in the following. When the HF etching reaction was finished, the sample was allowed to rest for 6 h and subsequently, the HF supernatant was recovered for recycling; 6 mL was recovered when 10 mL HF solution was used to etch 1 g of Ti_3AlC_2, and 4 mL fresh HF solution was replenished for the next etching reaction until the HF solution was recycled. All the HF waste was collected and treated with $CaCO_3$/$CaCl_2$ (1 : 4, wt%) to form stable CaF_2 precipitation. For example, $CaCO_3$/$CaCl_2$ was slowly added to 200 mL HF waste with stirring until pH 10.0; all the reactions were conducted in the fume cupboard to avoid leaking HF that can cause damage to the environment and the human body.

Exfoliation of multi-layer $Ti_3C_2T_x$ into $Ti_3C_2T_x$ nanosheets

The as-obtained $Ti_3C_2T_x$ (0.3 g) after HF etching was magnetically stirred in 5 mL dimethyl sulfoxide/water (DMSO/H_2O = 1/4 vol/vol) for 12 h at room temperature. The DMSO pretreated solution was separated by centrifugation at 4000 rpm and the sediment powder was dispersed in 30 mL of deionized water in an ultrasonic bath for 2 h. Analogous to DMSO treatment, the control sample was treated with 0.3 g $Ti_3C_2T_x$ powder dispersed in 30 mL deionized water directly.

Device fabrication

The ITO glass was cleaned by ultra-sonication in detergent, deionized water, acetone, and isopropyl alcohol, sequentially, for 15 min each. After drying by blowing air, the cleaned ITO substrates were treated with plasma for 15 min to remove organic residues. The prepared SnO_2 precursor (diluted by water with SnO_2/H_2O = 1/3, v/v) was spin-coated onto the ITO substrate at 5000 rpm for 30 s, followed by thermal annealing at 150 °C for 30 min in ambient air. The cooled ITO/SnO_2 films were spin-coated with $Ti_3C_2T_x$ suspension in an aqueous solution at 4000 rpm for 30 s in a fuming cupboard. Next, 70 μL of mixed cation perovskite precursor with the formula $Cs_{0.05}$-$FA_{0.8}MA_{0.15}Pb(I_{087}Br_{0.13})_3$ (1.2 M) was dissolved in 1 mL of a mixed solvent of DMF and DMSO (DMF/DMSO = 4/1, v/v). The solvent was then spin-coated onto ITO/SnO_2 by two consecutive spin-coating steps (1000 rpm 5 s and 5000 rpm 20 s). During the spin-coating process, 120 μL of CB was poured onto the perovskite film at 15 s. The perovskite film was then annealed at 60 °C for 10 min and 100 °C for 40 min. The hole transporting layer

(P3HT) was deposited onto the top of the perovskite film at 4000 rpm for 30 s with the composition of 20 mg P3HT in CB solution. Finally, 60 nm of Au was thermally evaporated as a back electrode.

Results and discussion

Preparation of 2D $Ti_3C_2T_x$ from bulk Ti_3AlC_2

It is well known that stripping Al from Ti_3AlC_2 is carried out by the HF reaction *via* the breaking of the metal bond between Al and Ti_3C_2 in the ternary metal (eqn S(1)†). The fluoride ions and hydrogen bond resides in the Al vacancies that construct the 2D $Ti_3C_2T_x$. The 2D MXene was redispersed in DMSO/H_2O solution with vigorous stirring or ultrasound treatment to produce $Ti_3C_2T_x$ nanosheets. The preparation of $Ti_3C_2T_x$ nanosheets is depicted in Fig. 1a, which provides a convenient route for the production of 2D $Ti_3C_2T_x$ at the lab scale. After exfoliation, the 2D structure of $Ti_3C_2T_x$ was obtained with the surface randomly covered with –F, =O, and –OH terminal groups, which are of significance as active sites for interface passivation and catalysis. Given that NH_4F/HCl and LiF/HCl act as HF sources, herein, various fluoride compounds like HF, NH_4F/HCl and LiF/HCl were employed to selectively strip Al to produce 2D $Ti_3C_2T_x$. Fig. 1b shows the SEM images of the bulk and accordion-like morphologies obtained by etching with LiF/HCl, NH_4F/HCl and HF. Compared with the pristine SEM image from Ti_3AlC_2, the LiF/HCl and NH_4F/HCl etchants only modified the surface, not the internal structure to obtain the 2D morphology. However, the accordion-like structure was observed with HF etching from commercial bulk Ti_3AlC_2. To further confirm the structure of 2D $Ti_3C_2T_x$, we also obtained XRD patterns with various agents. Characteristic $Ti_3C_2T_x$ peaks were observed at 2θ = 9.02°, 18.19° and 27.59°, corresponding to (002) (004) and (006) crystal planes, in agreement with previous reports (2D Ti_3C_2, SCPDS#00-052-0875).[41] The (002) peak at 9.02° indicated

the d-spacing of ~0.9 nm based on Bragg's law (eqn S(2)†). It should be noted that peaks at 36.08°, 41.68°, 60.48°, 72.45° and 76.52° are related to the bulk Ti_3C_2 by-product from the etching process (bulk Ti_3C_2, SCPDS#03-065-8808). Bulk Ti_3C_2 can be separated with the further exfoliation of multilayer $Ti_3C_2T_x$ because it cannot be delaminated and therefore remains in the sediment with minimal effect on our final product, $Ti_3C_2T_x$ nanosheets.

To evaluate the effect of HF etching time, the batch method with different reaction times was employed as shown in Fig. 2. The morphology of the as-obtained samples was investigated by SEM images with reaction time increasing from 6 h to 36 h. The images in Fig. 2a show the accordion-like morphology under HF etching. With the increasing reaction time, the layer structure extended from the surface to the internal across the $Ti_3C_2T_x$ crystal, opening up to different degrees due to interfacial tension on exposure to the air. However, the distance between layers became compact due to the increment in surface defects with prolonging the reaction time to 36 hours. The XRD patterns also revealed feature peaks at 9.02°, 18.19°, and 27.59°, in agreement with 2D $Ti_3C_2T_x$. In Fig. 2b, bulk Ti_3AlC_2 remained within 6 hours of etching, indicating that the reaction time was insufficient to strip Al element from Ti_3AlC_2. Considering both the XRD pattern and the SEM image, it was concluded that the appropriate etching time was 12 hours, accounting for efficiency and productivity.

Recycling and disposal of HF solution

The toxicity of HF solution haunts the deployment of 2D $Ti_3C_2T_x$ on a large scale. It is necessary to reuse the HF etchant, which can significantly reduce HF waste disposal. As shown in Fig. 3, the recycling of the HF agent was carried out by reusing the HF solution for the next batch for an increasing number of cycles. On recycling the HF solution 5 times, the separation of $Ti_3C_2T_x$ out of tHe F solution by centrifugation became difficult. It
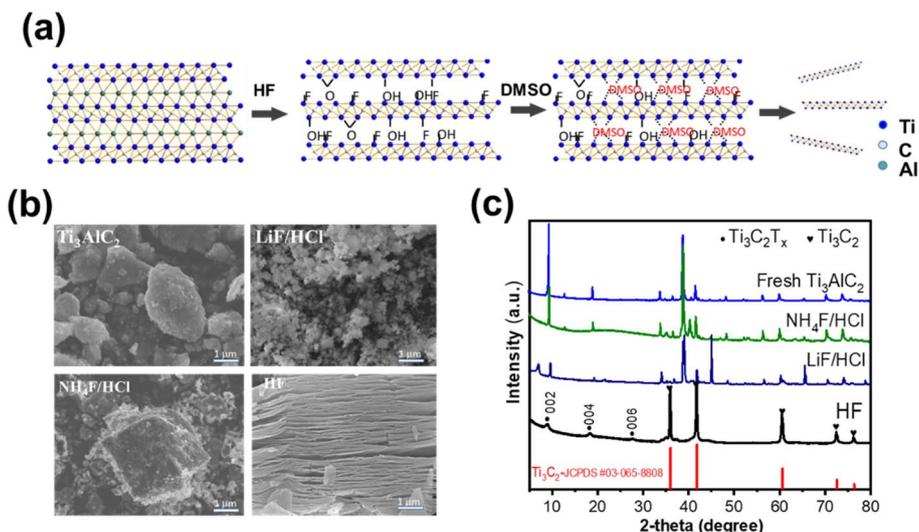

Fig. 1 (a) The illustration of the preparation of 2D $Ti_3C_2T_x$. (b) SEM images and (c) XRD patterns of $Ti_3C_2T_x$ after HF, LiF/HCl and NH_4F/HCl etching, respectively.
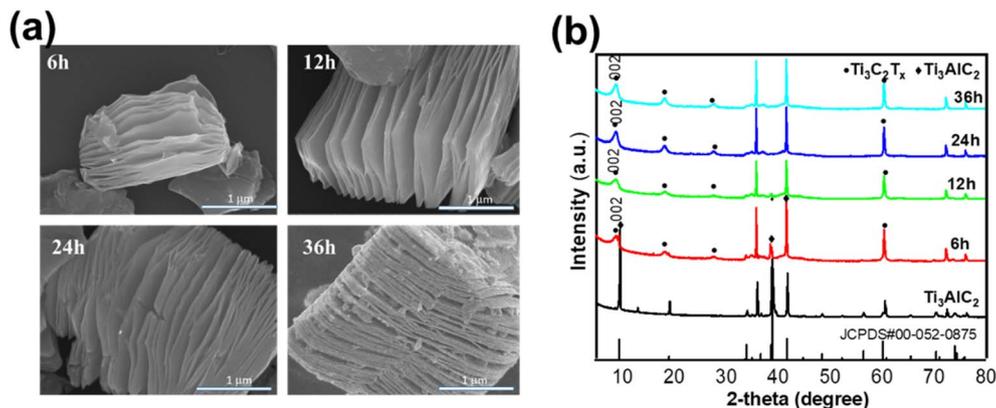
Fig. 2 (a) Variation of SEM images and (b) XRD patterns of $Ti_3C_2T_x$ with HF etching time.
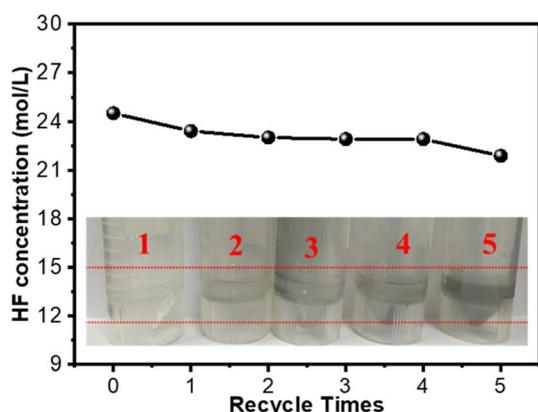

Fig. 3 The concentration of HF solution with the number of recycles. Inset: the evolution of the color change in centrifuge tubes.

should be noted that the concentration of HF showed a minimal decrease from the original 24.5 mol L^{-1} to 21.9 mol L^{-1}, whereas the accumulation of impurities including AlF_3 and Ti_3C_2 resulted in the limitation of the recycling of HF. As revealed in Fig. 3, the darkening of the HF solution with the number of recycling processes indicated the accumulation of impurities. More importantly, hazardous HF waste is one of the key issues to an environmentally friendly approach. Therefore, we provided low-cost $CaCO_3/CaCl_2$ to precipitate CaF_2 ($K_{sp} = 3.4 \times 10^{-11}$ at 20 °C) for the disposal of HF sewage. $CaCl_2$ was also employed to alleviate the severe reaction due to neutralization heating. As a result, the concentration of fluoride in HF waste was determined by ion chromatography (IC) to be 5.35 mg L^{-1} after the CaF_2 reaction. The harmful HF waste was minimized through a facile operation according to the China regulation of sewage discharge (GB8978-1996), which was expected to produce 2D $Ti_3C_2T_x$ on a large scale without the limitations of the toxic HF solution.

DMSO-assisted exfoliation of $Ti_3C_2T_x$

As illustrated in Fig. 4, the stable $Ti_3C_2T_x$ suspension with a unique smell was obtained *via* DMSO treatment in an aqueous

solution (1/4, vol/vol). $Ti_3C_2T_x$, assisted by DMSO, can be easily delaminated into nanosheets in an ultrasonic bath, due to the function of DMSO located at the interface with a strong bond between DMSO and terminal groups. Compared to DMSO treatment, a poor exfoliation effect was observed in pure aqueous solutions, largely ascribed to the weak coupling of hydrogen bonds and terminal groups at the interface. As shown in Fig. 4a, the SEM of $Ti_3C_2T_x$ nanosheets by DSMO-assisted exfoliation was spotted in SEM images, which presented the single-layer feature of 2D $Ti_3C_2T_x$. Under TEM images in Fig. 4b, the distance of the (002) plane was determined to be 0.9 nm, which is in accordance with the value determined by XRD. In addition, the nanosheet size distribution was determined by SEM images and dynamic light scattering (DLS) in Fig. 4a and c. The size of exfoliated $Ti_3C_2T_x$ nanosheets ranged from 150 nm to 300 nm. The Ti_3C_2 nanosheets exhibited superconductivity due to the coupling of terminal groups (–F, =O, *etc.*), which is comparable to the metal. The MXene nanosheets showed the features of conductors, with a sheet resistance of 5500 S cm^{-1} in agreement with previous reports. It should be noted that the suspension was unstable when kept in an aqueous solution for a long time as revealed in Fig. S1,† where the size distribution ranged from 300 nm to 1000 nm after 10 days of storage. This phenomenon reminds us that the 2D $Ti_3C_2T_x$ suspension should be kept at a low temperature and used while fresh.

Passivation of the perovskite/electron transfer interface with $Ti_3C_2T_x$ nanosheets

The interface plays a crucial role in determining the performance of perovskite working devices. The $Ti_3C_2T_x$ nanosheet is introduced to passive the perovskite/electron transport layer (ETL) due to its functional terminal groups (–F, –OH or =O). As shown in Fig. 5a, the single-layer $Ti_3C_2T_x$ was deposited on SnO_2 ETL, which can couple with perovskite with terminal groups and thus promote the growth of perovskite crystals. The PL intensity of the perovskite exhibited a two-fold increment with $Ti_3C_2T_x$ interfacial passivation as compared to the control perovskite film, indicating the reduction of non-radiative recombination at the interface (Fig. 5b). We also performed time-resolved PL (TRPL) studies to support the recombination
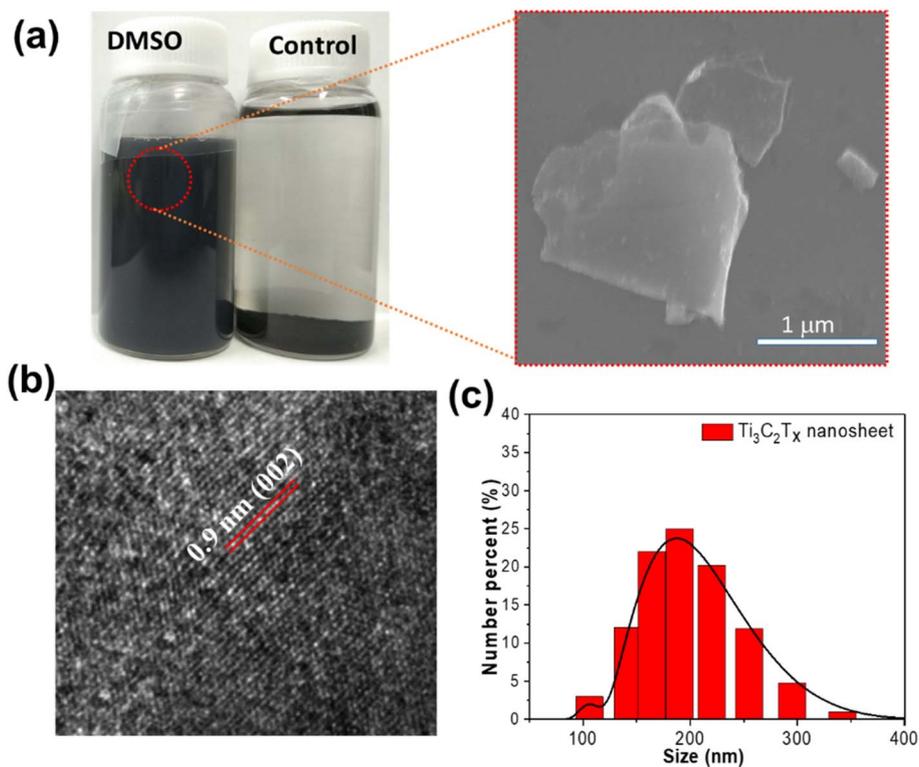
Fig. 4 (a) The suspension of $Ti_3C_2T_x$ in DMSO/H_2O and aqueous solution, respectively. Inset: the SEM image of a $Ti_3C_2T_x$ single layer on a silicon wafer. (b) TEM image and (c) the size distribution of the $Ti_3C_2T_x$ nanosheets.

of the photogenerated carriers. Fig. S5† shows that the Ti_3C_2 nanosheet passivated film displayed a longer average carrier lifetime (t_{ave} ~75.03 μs) than the control sample (t_{ave} ~63.56 μs). The high carrier lifetime at the Ti_3C_2/perovskite interface is in favor of the charge transfer and effective suppression of defects-induced recombination at the interface, contributing to higher
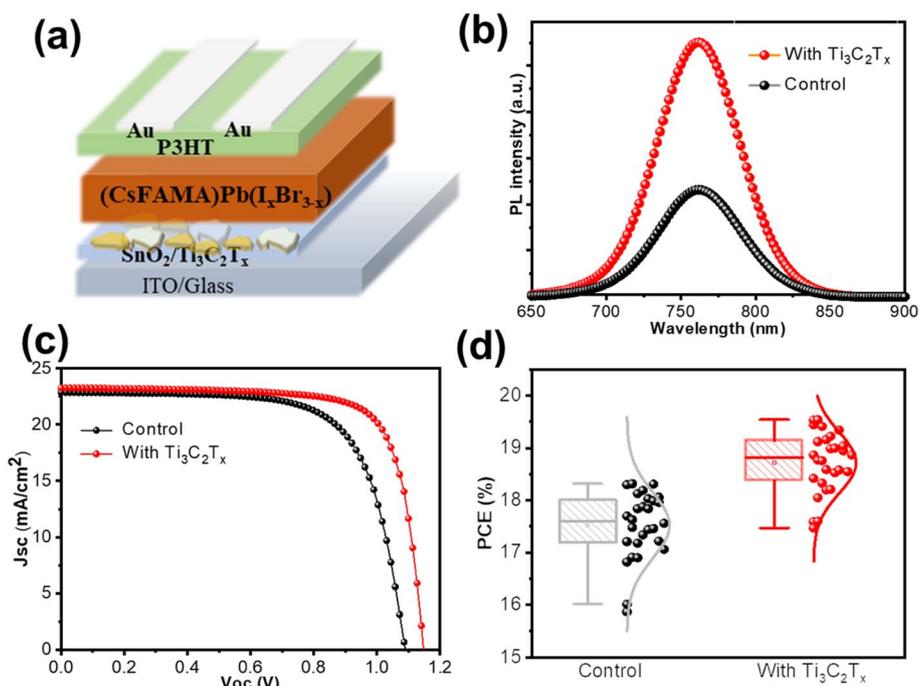

Fig. 5 (a) Schematic diagram of the perovskite solar device. (b) PL spectra of the control and passivated perovskite films. (c) J–V curves of the perovskite working device and (d) the PCEs distribution of perovskite solar cells.

efficiency and V_{OC} values. The cross-section images of perovskite films in Fig. S3† also display the conformity of perovskite crystals based on the ITO/SnO$_2$/Ti$_3$C$_2$T$_x$ substrate. In addition, the ITO/SnO$_2$ substrate with Ti$_3$C$_2$T$_x$ exhibited a high transmittance of around 70%, ranging from 300 nm to 800 nm in Fig. S2,† owing to the high transparency of the single-layer 2D Ti$_3$C$_2$T$_x$ nanosheet. More importantly, the secondary electron cutoff for the Ti$_3$C$_2$-modified SnO$_2$ was 16.81 eV. The corresponding work function calculated by subtracting secondary electron cutoffs from the excitation energy for Ti$_3$C$_2$-modified SnO$_2$ was 4.35 eV. As depicted in Fig. S6,† the work function of Ti$_3$C$_2$-modified SnO$_2$ can form a better cascade-type energy-level alignment with the perovskite layer, which facilitates more efficient charge extraction, thereby reducing the energy loss of the photon-generated holes transferred from the perovskite to the electron transport film. As a result, the perovskite device with a composition of Cs$_{0.05}$FA$_{0.8}$MA$_{0.15}$Pb(I$_{0.87}$Br$_{0.13}$)$_3$ in n–i–p planar configuration was fabricated, which demonstrated a control efficiency (PCE) of 18.22% from the reverse scan, along with an open-voltage (V_{OC}) of 1.08 V, short-circuit current (J_{SC}) of 22.51 mA cm^{-2}, and fill factor (FF) of 0.75. Fig. 5c shows a champion efficiency of 20.33% after interfacial passivation, giving a V_{OC} of 1.15 V, J_{SC} of 22.87 mA cm^{-2}, and FF of 0.78. Interestingly, the enhancement of V_{OC} to 1.15 V was realized by depositing a thin Ti$_3$C$_2$T$_x$ nanosheet atop SnO$_2$, due to the passivation of interfacial defects with minimal energy loss. Additionally, the current density (J_{int}) by integration of the EQE spectra under 1 sun is in agreement with the values from the J–V curve (Fig. S4†). The corresponding PCE distribution is summarized in Fig. 5d, where the average PCE of the control device was 17.52%. However, in comparison to the control device, the optimal device with Ti$_3$C$_2$T$_x$ passivation presented an average PCE of 19.11% with a noticeable 9% enhancement. The data were collected from ∼30 solar cells for each device. The overall enhancement of PCE typifies the effectiveness of Ti$_3$C$_2$T$_x$ passivation due to its abundant terminal groups. In addition, we investigated the long-term stability of the devices under socking, storing them in the atmosphere without any encapsulation (Fig. S7†). The control devices underwent a gradual efficiency decline during the 350 hours of tracking, retaining 40% of their initial efficiency. In comparison, the device processed from the Ti$_3$C$_2$ passivation preserved 80% initial efficiency for the entire light socking within 350 hours of testing. The employment of 2D Ti$_3$C$_2$T$_x$ in perovskite devices provides a guide for the application of 2D materials, taking advantage of its environment-friendly production.

Conclusions

We have presented a universal low-cost and environment-friendly approach to preparing 2D Ti$_3$C$_2$T$_x$ from commercial Ti$_3$AlC$_2$ powder, and integrated a process including the exfoliation of Ti$_3$C$_2$T$_x$, hazardous HF etchant disposal, and stable storage of Ti$_3$C$_2$T$_x$ nanosheets. SEM showed that the 2D Ti$_3$C$_2$T$_x$ obtained *via* HF etching exhibited an accordion-like morphology. The DMSO-assisted exfoliation process was also investigated, indicating that DMSO cooperates with terminal groups at the interface to promote the exfoliation of Ti$_3$C$_2$T$_x$. More importantly, the hazardous HF waste solution was disposed of based on the reaction with CaCO$_3$/CaCl$_2$ to precipitate CaF$_2$. The reproducible Ti$_3$C$_2$T$_x$ nanosheets were deposited at the interface in the perovskite solar device with enhanced efficiency, advancing the development of its applications. Ti$_3$C$_2$ works efficiently for perovskite solar devices, increasing the PCE by ∼9% with a V_{OC} of up to 1.15 V. The effect of Ti$_3$C$_2$ on perovskite passivation has been discussed in this work in detail. The interface modification was introduced for the deposition of perovskite thin films for advancing their large-scale deployment.

Author contribution

Qingchao Shen is the founder of this work; Chaoran Chen, Jiao Long, and Saili Wang contribute equally to revise this paper.

Conflicts of interest

There are no conflicts to declare.

Acknowledgements

References

1 M. Ghidiu, M. R. Lukatskaya, M. Zhao, Y. Gogotsi and M. W. Barsoum, Conductive two-dimensional titanium carbide 'clay' with high volumetric capacitance, *Nature*, 2014, **516**, 78–81.

2 M. Naguib, O. Mashtalir, J. Carle, V. Presser, J. Lu, L. Hultman, Y. Gogotsi and M. W. Barsoum, Two-Dimensional Transition Metal Carbides, *ACS Nano*, 2012, **6**(2), 1322–1331.

3 M. Naguib, V. N. Mochalin, M. W. Barsoum and Y. Gogotsi, 25th Anniversary Article: MXenes: A New Family of Two-Dimensional Materials, *Adv. Mater.*, 2014, **26**, 992–1005.

4 M. Khazaei, A. Ranjbar, M. Arai, T. Sasaki and S. Yunoki, Electronic properties and applications of MXenes: a theoretical review, *J. Mater. Chem. C*, 2017, **5**, 2488–2503.

5 B. Anasori, Y. Xie and M. Beidaghi, Two-dimensional, ordered, double transition metals carbides (MXenes), *ACS Nano*, 2015, **9**(10), 9507–9516.

6 N. K. Chaudhari, H. Jina, B. Kima, D. S. Baekc, S. H. Jooc and K. Lee, MXene: An Emerging Two-Dimensional Material for Future Energy Conversion and Storage Applications, *J. Mater. Chem. A*, 2017, **5**, 24564–24579.

7 R. Li, L. Zhang, L. Shi and P. Wang, MXene Ti$_3$C$_2$: An Effective 2D Light-to-Heat Conversion Material, *ACS Nano*, 2017, **11**, 3752–3759.

8 N. J. Alvarez, E. C. Kumbur and Y. Gogotsi, Rheological Characteristics of 2D Titanium Carbide (MXene)

Dispersions: A Guide for Processing MXenes, *ACS Nano*, 2018, **12**, 2685–2694.

9 C. Zhang, M. Beidaghi, M. Naguib, M. R. Lukatskaya, M. Zhao, B. Dyatkin, K. M. Cook, S. J. Kim, B. Eng, X. Xiao, D. Long, W. Qiao, B. Dunn and Y. Gogotsi, Synthesis and Charge Storage Properties of Hierarchical Niobium Pentoxide/Carbon/Niobium Carbide (MXene) Hybrid Materials, *Chem. Mater.*, 2016, **28**, 3937–3943.

10 A. Lipatov, M. Alhabeb, R. Lukatskaya, A. Boson, Y. Gogotsi and A. Sinitskii, Effect of Synthesis on Quality, Electronic Properties and Environmental Stability of Individual Monolayer Ti$_3$C$_2$ MXene Flakes, *Adv. Bioelectron. Mater.*, 2016, **2**, 1600255.

11 M. Alhabeb, K. Maleski, B. Anasori, P. Lelyukh, L. Clark, S. Sin and Y. Gogotsi, Guidelines for Synthesis and Processing of Two-Dimensional Titanium Carbide (Ti$_3$C$_2$T$_x$ MXene), *Chem. Mater.*, 2017, **29**, 7633–7644.

12 S. Niu, Z. Wang, M. Yu, M. Yu, L. Xiu, S. Wang, X. Wu and J. Qiu, MXene-Based Electrode with Enhanced Pseudocapacitance and Volumetric Capacity for Power-Type and Ultra-Long Life Lithium Storage, *ACS Nano*, 2018, **12**(4), 3928–3937.

13 Y. Wang, H. Dou, J. Wang, B. Ding, Y. Xu, Z. Chang and X. Hao, Three-dimensional porous MXene/layered double hydroxide composite for high performance supercapacitors, *J. Power Sources*, 2016, **327**, 221–228.

14 M. R. Lukatskaya, S. Kota, Z. Lin, M. Zhao, N. Shpigel, M. D. Levi, J. Halim, P. Taberna, M. W. Barsoum, P. Simon and Y. Gogotsi, Ultra-high-rate pseudocapacitive energy storage in two-dimensional transition metal carbides, *Nat. Energy*, 2017, **2**, 17105–17110.

15 C. Zhang, M. P. Kremer, A. Seral-Ascaso, S. Park, N. McEvoy, B. Anasori, Y. Gogotsi and V. Nicolosi, Stamping of Flexible, Coplanar Micro-Supercapacitors Using MXene Inks, *Adv. Funct. Mater.*, 2018, 1705506.

16 Y. Dong, S. Zheng, J. Qin, X. Zhao, H. Shi, X. Wang, J. Chen and Z. Wu, All-MXene-Based Integrated Electrode Constructed by Ti$_3$C$_2$ Nanoribbon Framework Host and Nanosheet Interlayer for High Energy-Density Li-S Batteries, *ACS Nano*, 2018, **12**(3), 2381–2388.

17 A. V. Mohammadi, A. Hadjikhani, S. Shahbazmohamadi and M. Beidaghi, Two-Dimensional Vanadium Carbide (MXene) as a High Capacity Cathode Material for Rechargeable Aluminum Batteries, *ACS Nano*, 2017, **11**(11), 11135–11144.

18 Y. Wu, P. Nie, L. Wu, H. Dou and X. Zhang, 2D MXene/SnS$_2$ composites as high-performance anodes for sodium ion batteries, *Chem. Eng. J.*, 2018, **334**, 932–938.

19 Y. Wu, P. Nie, J. Wang, H. Dou and X. Zhang, Few-Layer MXenes Delaminated via High-Energy Mechanical Milling for Enhanced Sodium-Ion Batteries Performance, *ACS Appl. Mater. Interfaces*, 2017, **9**(45), 39610–39617.

20 H. Zhang, Z. Fua, R. Zhanga, Q. Zhanga, H. Tiana, D. Legutc, T. C. Germannd, Y. Guoa, S. Due and J. S. Francisco, Designing flexible 2D transition metal carbides with strain-controllable lithium storage, *PANS*, 2017, **10**, 326–328.

21 C. Chen, X. Xie, B. Anasori, A. Sarycheva, T. Makaryan, M. Zhao, P. Urbankowski, L. Miao, J. Jiang and Y. Gogotsi,

MoS$_2$-on-MXene heterostructures as highly reversible anode materials for lithium-ion batteries, *Angew. Chem.*, 2018, **130**, 1864–1868.

22 Z. Wang, H. Kim and H. N. Alshareef, Oxide Thin-Film Electronics using All-MXene Electrical Contacts, *Adv. Mater.*, 2018, **30**, 1706656.

23 M. Marianoa, O. Mashtalirb, F. Q. Antonio, W. Ryu, B. Deng, F. Xia, Y. Gogotsi and A. D. Taylor, Solution-processed Titanium Carbide MXene films examined as highly transparent conductors, *Nanoscale*, 2016, **10**, 1–8.

24 X. Chen, X. Sun, W. Xu, G. Pan, D. Zhou, J. Zhu, H. Wang, X. Bai, B. Dong and H. Song, Ratiometric Photoluminescence Sensing based on Ti$_3$C$_2$ MXene Quantum Dots for the Intracellular pH Sensor, *Nanoscale*, 2018, **10**, 1111–1118.

25 C. Yeon, S. J. Yun, J. Yang, D. Youn and J. W. Lim, Na-Cation-Assisted Exfoliation of MX$_2$ (M = Mo, W; X = S, Se) Nanosheets in an Aqueous Medium with the Aid of a Polymeric Surfactant for Flexible Polymer-Nanocomposite Memory Applications, *Small*, 2017, 1702747.

26 Y. Cai, J. Shen, G. Ge, Y. Zhang, W. Jin, W. Huang, J. Shao, J. Yang and X. Dong, Stretchable Ti$_3$C$_2$T$_x$ MXene/Carbon Nanotubes Composite Based Strain Sensor with Ultrahigh Sensitivity and Tunable Sensing Range, *ACS Nano*, 2018, **12**(1), 56–62.

27 M. Zhao, M. Sedran, Z. Ling, M. R. Lukatskaya, O. Mashtalir, M. Ghidiu, B. Dyatkin, D. J. Tallman, T. Djenizian, M. W. Barsoum and Y. Gogotsi, Synthesis of Carbon/Sulfur Nanolaminates by Electrochemical Extraction of Titanium from Ti$_2$SC, *Angew. Chem., Int. Ed.*, 2015, **54**, 4810–4814.

28 Z. Xu, Y. Sun, Y. Zhuang, W. Jing, H. Ye and Z. Cui, Assembly of 2D MXene Nanosheets and TiO$_2$ Nanoparticles for Fabricating Mesoporous TiO$_2$-MXene Membranes, *J. Membr. Sci.*, 2018, **12**, 3928–3937.

29 L. Ding, Y. Wei, L. Li, T. Zhang, H. Wang, J. Xue, L. Ding, S. Wang, J. Caro and Y. Gogotsi, MXene molecular sieving membranes for highly efficient gas separation, *Nat. Commun.*, 2018, **9**, 155.

30 R. Bian, R. Lin, G. Wang, G. Lu, W. Zhi, S. Xiang, T. Wang, P. S. Clegg, D. Cai and W. Huang, 3D assembly of Ti$_3$C$_2$-MXene directed by water/oil interfaces, *Nanoscale*, 2018, **10**, 116–121.

31 N. K. Chaudharia, H. Jina, B. Kima, D. S. Baekc, S. H. Jooc and K. Lee, MXene: An Emerging Two-Dimensional Material for Future Energy Conversion and Storage Applications, *J. Mater. Chem. A*, 2017, **5**, 24564–24579.

32 H. Lin, Y. Wang, S. Gao, Y. Chen and J. Shi, Theranostic 2D Tantalum Carbide (MXene), *Adv. Mater.*, 2017, 1703284.

33 X. Li, X. Yin, M. Han, C. Song, X. Sun, H. Xu, L. Cheng and L. Zhang, Controllable heterogeneous structure and electromagnetic wave absorption properties of Ti$_2$CT$_x$ MXene, *J. Mater. Chem. C*, 2017, **5**, 7621–7628.

34 X. Wang, C. Garnero, G. Rochard, D. Magne, S. Morisset, S. Hurand, P. Chartier, J. Rousseau, T. Cabioc'h, C. Coutanceau and V. M. S. Célérier, New etching environment (FeF$_3$/HCl) for the synthesis of two dimensional titanium carbide MXenes: a route towards

selective reactivity vs. water, *J. Mater. Chem. A*, 2017, **5**, 22012–22023.

35 T. Zhang, L. Pan, H. Tang, F. Du, Y. Guo, T. Qiu and J. Yang, Synthesis of two-dimensional $Ti_3C_2T_x$ MXene using HCl/LiF etchant: Enhanced exfoliation and delamination, *J. Alloys Compd.*, 2017, **695**, 818–826.

36 W. Suna, S. A. Shaha, Y. Chenb, Z. Tanb, H. Gaob, T. Habiba, M. Radovic and M. J. Green, Electrochemical etching of Ti_2AlC to Ti_2CT_x (MXene) in low concentration hydrochloric acid solution, *J. Mater. Chem. A*, 2017, **5**, 21663–21668.

37 S. Laia, J. Jeona, S. K. Janga, J. Xua, Y. J. Choic, J. Parkd, E. Hwanga and S. Lee, Surface group modification and carrier transport property of layered transition metal carbides (Ti_2CT_x, T: –OH, –F and –O), *Nanoscale*, 2015, **7**, 19390–19396.

38 L. Lia, F. Wang, J. Zhu and W. Wu, Facile Synthesis of Layered Ti_2C MXene/Carbon Nanotube Composite Paper with Enhanced Electrochemical Property, *Dalton Trans.*, 2017, **10**, 1035–1040.

39 W. Yuan, L. Cheng, Y. Zhang, H. Wu, S. Lv, L. Chai, X. Guo and L. Zheng, 2D-Layered Carbon/TiO_2 Hybrids Derived from Ti_3C_2 MXenes for Photocatalytic Hydrogen Evolution under Visible Light Irradiation, *Adv. Mater. Interfaces*, 2017, 1700577.

40 F. Wang, C. Yang, M. Duan, Y. Tang and J. Zhu, TiO_2 nanoparticle modified organ-like Ti_3C_2 MXene nanocomposite encapsulating hemoglobin for a mediator-free biosensor with excellent performances, *Biosens. Bioelectron.*, 2015, **74**, 1022–1028.

41 M. Ghidiu, J. Halim, S. Kota, D. Bish, Y. Gogotsi and M. W. Barsoum, Ion-Exchange and Cation Solvation Reactions in Ti_3C_2 MXene, *Chem. Mater.*, 2016, **28**, 3507–3514.